

Synthesis and characterization of Al-Ag/ZnO nano-photocatalyst for dye degradation in newly designed multi-layer cylindrical photoreactor

Bahman ZareNezhad ¹, Mohammad Reza Khodadadi ², Mohammad Ebrahim Olya ^{3,*}

¹ Faculty of Chemical, Petroleum and Gas Engineering, Semnan University, Semnan, Iran

² Department of Nanotechnology, Semnan University, Semnan, Iran

³ Department of Environmental Research, Institute for Color Science and Technology, P.O. Box 16765-654, Tehran, Iran

Abstract: A new Ag-Al/ZnO nano-photocatalyst has been synthesized by doping technique for degradation of Reactive Blue 19 (RB19) under UV irradiation. The photocatalytic activity of the synthesized nanocatalyst has been investigated in a newly designed multi-layered cylindrical reactor. The Al-Ag/ZnO nano-photocatalyst has much more photocatalytic activity as compared to the ZnO and Ag/ZnO at similar operating conditions. It is found that the photocatalytic degradation using the newly synthesized nano-photocatalyst follows pseudo first order kinetic model. The electrical energy consumption with the nano-photocatalyst used in this work is much lower than that in the other alternative processes.

Keywords: Nano-photocatalyst; Reactor; Degradation; Wastewater treatment; Kinetics study.

Introduction

Environmental effects of synthetic dyes that are consumed in chemical industries have important issues which need to be under serious consideration. Most dyes pollutions come from textile wastewater ^{1,2} and about 10-20 % of dyes are directed to the rivers ³. Different methods are used for wastewater purification such as chemical, physical, and biological operations. Recent developments in the domain of chemical water treatment have led to an improvement in oxidative degradation procedures to remove organic materials in wastewater by oxidation through catalytic and photochemical methods. They are generally referred to as advanced oxidation processes (AOPs) which are chemical treatment methods for degradation of organic components from water ^{4,5}. In AOPs techniques, generation of the hydroxyl radicals (OH[•]) has an important role in oxidation and degradation of dye components to simple mineral ingredients ^{2,6}. One of the best oxidation processes is photocatalytic degradation of organic compounds using special photo sensitive catalysts such as TiO₂ or ZnO under ultraviolet (UV) or light irradiation ^{7,8}. ZnO is a donor transition classified as an n-type semiconductor. Its admirable features like thermal stability and high transparency make it a valuable material for photocatalysis, chemical sensors, gas sensors, biosensors, solar cells, electrochemical cells, electrical and optical devices. Moreover, the band gap of ZnO is about 3.37 eV at room temperature ⁹

with electron mobility around 115-155 cm²V⁻¹S⁻¹ which is comparable to TiO₂ photocatalyst ¹⁰. There are different papers regarding doping materials such as Mg ¹¹, Cd ¹², Sn ¹³, Al ¹⁴ and Ag with ZnO. It is reported that an increase in Ag concentration increases the photocatalytic activity of ZnO ¹⁵. Ahmad et al. have improved the synthesis of Al/ZnO (AZO) with combustion method and found maximum band gap in the range of 3.12 to 3.21 eV with different aluminum molar concentrations (0.5-6.0%) ^{16,17}.

Various methods have been used for ZnO crystal growth such as sol-gel technique ¹⁸, pulsed laser deposition ¹⁹, plasma-assisted approach ²⁰, thermal CVD ²¹ and hydrothermal process ²². Many of the aforementioned synthetic methods use structure directing agents for the morphology and properties improvement. Different morphology of ZnO have been reported, nanoflowers ²³, quasi spherical ²⁴, nanogranule ²⁵, capsule like ²⁶, nano ribbons, nano tubes and etc. Each of the mentioned morphology has its own significance for the catalytic and industrial applications ²⁷. All of the aforementioned methods can be used to incorporate an impurity in ZnO crystal structure.

However the unfavorable high synthesis temperature and serious technical complications are challenging matters. Recently, the application of microwave energy with the solution combustion reaction for synthesis of powders is introduced ²⁸. Because of the low cost, energy saving and reduced processing time, the microwave technique has got

*Corresponding author: Mohammad Ebrahim Olya

E-mail address: olya-me@icrc.ac.ir

DOI: <http://dx.doi.org/>

wide applications in material synthesis^{29,30}. Moreover, in the chemical industry it is preferred to use the continuous operation in dealing with large quantities of materials³¹. Semi-continuous reactors as a lab equipment seem to be specifically suited for achieving degradation of dyes. Most of the earlier studies have been conducted in batch reactors using dye solutions and very few reports are available on treatment in semicontinuous reactors.

In this study, Ag and Al doping materials have been incorporated in the ZnO nanoparticle and the resulting nano-photocatalyst (Ag-Al/ZnO) has been synthesized, characterized and tested in a new multi-layered cylindrical photoreactor. The photocatalytic activity of the synthesized nanocatalyst is examined by photo-degradation of Reactive Blue 19 (RB19); a toxic wastewater dye widely used in wool textile, food and cosmetics; as a representative toxic dye in industrial wastewater, under UV irradiation in a new designed multi-layered cylindrical reactor. To the extent of our knowledge, there are few papers that talk about synthesis of Ag and Al co doped ZnO regarding to degradation of RB19.

Experimental Section

Materials

Zinc nitrate hexahydrate ($\text{Zn}(\text{NO}_3)_2 \cdot 6\text{H}_2\text{O}$), Silver nitrate (AgNO_3), Aluminum nitrate ($\text{Al}(\text{NO}_3)_3$), glycine and glucose as the ingredients of the final products. Hydrogen peroxide (H_2O_2), H_2SO_4 and NaOH solutions are provided from Merck chemicals. The dye (Reactive Blue 19; C.I. 61200) which has been used for photocatalytic testing of Al-Ag/ZnO is purchased from Alvan Sabet chemical company (Tehran, Iran).

Synthesis of nano photocatalyst

Hydrothermal process with the assistance of microwave oven has been used to synthesize Ag-Al/ZnO. Zinc nitrate hexahydrate [$\text{Zn}(\text{NO}_3)_2 \cdot 6\text{H}_2\text{O}$ (Merck, 99.5%)], Aluminum nitrate nona hydrate, [$\text{Al}(\text{NO}_3)_3 \cdot 9\text{H}_2\text{O}$ (Merck, 99%)] and Silver nitrate [AgNO_3 (Merck, 99.8%)] have been used for the synthesis operation. About 5 g $\text{Zn}(\text{NO}_3)_2 \cdot 6\text{H}_2\text{O}$ and 0.2 g AgNO_3 were dissolved completely in deionized water at 25 °C. Stoichiometric amounts of glucose and glycine have been added as fuel solution. Different amounts of $\text{Al}(\text{NO}_3)_3 \cdot 9\text{H}_2\text{O}$ was added and stirred slowly to prepare level mixture. The mixture is heated to about 70-100 °C to avoid reaction before

a viscous gel appears. A beaker containing of provided gel was placed into a microwave oven (900 W, 2450 MHz, LG) and after 60 s of continuously irradiation, a foamy porous powder is obtained. The synthesized catalysts contain 7 mol% of Ag (related to ZnO) and set with 1, 3 and 8 mol% of Al (related to ZnO) respectively.

Photocatalytic reactor

All the experiments have been carried out in a multi-layered cylindrical photocatalytic reactor which has been designed by the authors as shown in Figure 1. The reactor layers are assembled with quartz glass to maximize the UV light transfer. For maximum irradiation, the reactor is covered with aluminum foil. An UV lamp (Osram Sylvania G15T8 15W 18" UV Germicidal Lamp) with the length of 420 mm is placed at the middle of the reactor to avoid contact with water solution. The total irradiated surface area and light distribution within the reactor can be optimized by adjusting the position of all cylinders³². The diameters of external, middle and internal quartz cylinders are about 85 mm, 75 mm and 65 mm respectively. The reactor is 400 mm long with the total internal volume of 1805 ml.

Appropriate amount of photocatalyst solution has been sonicated to decrease the particles size and increase the surface area of catalyst²⁸. The mixtures of catalyst and dye are circulated in the reactor. The UV lamp is turned on and 4 mL samples are taken at specific time intervals and centrifuged to separate the suspended catalyst particles. The RB19 concentration is measured with an UV-Vis spectrophotometer (Model: Perkin-Elmer lambda 25) and the amount of carbon bound is measured by TOC Analyzer (Shimadzu TOC-L CSH E200). The decolorization activity and mineralization percentage of organic compound can be calculated as follows:

$$\text{Decolorization efficiency} = \left(1 - \frac{A}{A_0}\right) \times 100 \quad (1)$$

$$\text{Mineralization percent} = \left(1 - \frac{\text{TOC}}{\text{TOC}_0}\right) \times 100 \quad (2)$$

Where A and A_0 are the dye concentration at time t and t=0 respectively and TOC and TOC_0 are total organic carbon at time t and t=0 respectively.

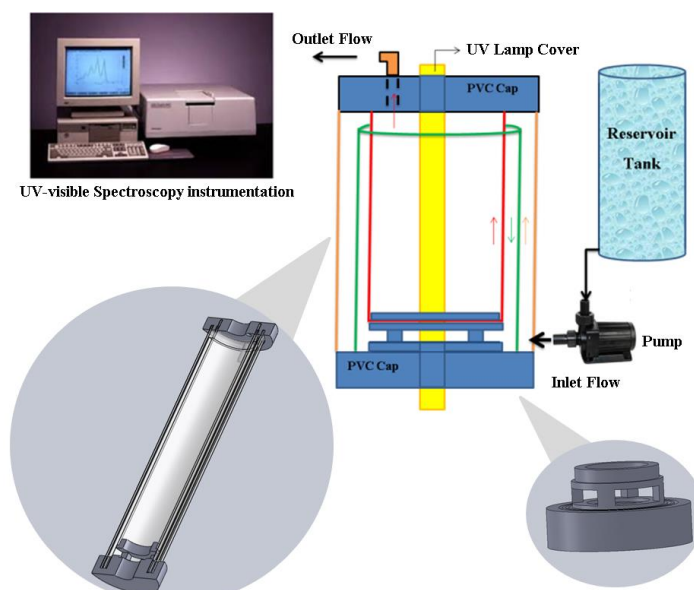


Figure 1. A schematic diagram of the designed photocatalytic reactor: Outer, middle and inner quartz cylinder in brown, green and red respectively. The UV lamp in yellow and the direction of the flow in each cylinder in colored arrows.

Analytical Methods

The composition of synthesized doped ZnO powder has been characterized by Fourier-transform infrared (FTIR) spectroscopy using a Perkin-Elmer spectrometer. X-Ray diffraction (XRD) patterns are performed at Cu-K α ($\lambda=1.54056 \text{ \AA}$) radiation with diffraction angle (2θ) range of 10° to 100° and a typical step size of 0.026° to identify crystalline phase. The surface morphology is observed with scanning electron microscopy technique (SEM) using the LEO 1455vp apparatus. Kinetics study of RB19 decolorization process and photocatalytic activity of treated ZnO have been investigated by ultraviolet-visible (UV-Vis) absorption double beam spectrophotometer (Perkin-Elmer lambda 25 Model) over a wavelength range of 200 nm to 800 nm.

Result and Discussion

Characterization

Characterizations of synthesized nano-photocatalyst by XRD, FTIR and SEM are presented in the following sections.

XRD Analysis

X-ray diffraction patterns of ZnO, Ag/ZnO and Ag-Al/ZnO are presented in Figure 2. The XRD peaks of ZnO correspond to an index card number (01-076-0704) suggesting the existence of wurtzite structure with hexagonal crystal lattice. The index peaks of ZnO can be noted as $31.7 - 34.4 - 36.25 - 47.5 - 56.6$ and 62.9 degrees that are related to (100), (002), (101), (102), (110), (103) surfaces. According to Scherer equation:

$$D = \frac{k\lambda}{\beta \cos\theta} \quad (3)$$

The calculated crystal lattice size of ZnO sample is about 45.7 nm. In Eq. (3), D is the average

crystallite size (nm), k is a constant equal to 0.89, λ is the X-ray wavelength equal to 0.154056 nm, β is the full width at half maximum intensity and θ is the half diffraction angle. Incorporation of silver nitrate into the ZnO structure leads to the formation of metallic silver as a minor phase (JCPDS card no: 01-080-0998) and the crystallite size is decreased to 43.6 nm due to the doping operation. Because of the limited solubility of silver ions in the zinc oxide structure, the creation of metallic silver and silver oxide peaks can be seen at 37.9° . Aluminum as a second dopant decreases the lattice size of Ag-Al/ZnO to about 42.4 nm. Increase in crystal size can be attributed to the limited solubility of Al^{3+} ions into the ZnO structure³⁵.

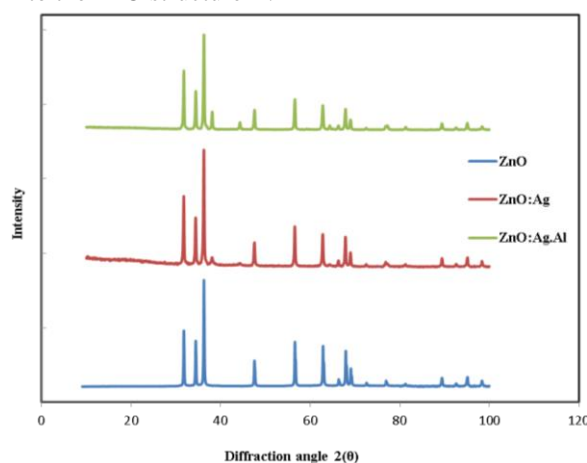


Figure 2. The XRD patterns of the pure ZnO, Ag/ZnO, Ag-Al co doped ZnO photocatalysts

FTIR Analysis

Doping of metals into zinc oxide changes the intensity of peaks as it can be seen in all samples (Figure 3). Therefore in all cases the peaks of 3000 cm^{-1} to 3440 cm^{-1} corresponding to the OH groups in a significant condition, produce an electron and a hole in the surface of ZnO. The electron transfers and reacts with free radicals available in the dye which leads to the photocatalytic oxidation of the dye ³⁶. The bands at 2900 cm^{-1} and 2930 cm^{-1} are attributed to C-H bending and stretching mode and the peaks around 2300 cm^{-1} relate to C-N bonding, which are related to the presence of glucose and glycine as fuels solution in synthesis procedure ^{37,38}. The broad absorption in the range of 1640 cm^{-1} is assigned to the bending vibration and stretching mode of water and hydroxyl groups on the surface of the samples. The peaks from 458 cm^{-1} to 467 cm^{-1} represent the stretching vibration of Zn-O in all cases ³⁹. On doping with silver, stronger and wider absorption bands are observed and shown in Figure 3(a) in the region of $\sim 723\text{ cm}^{-1}$ ⁴⁰.

The intensity of the peaks in the range of 1070 cm^{-1} - 1100 cm^{-1} in Figure 3b is related to the Al-O formed bonds ⁴¹.

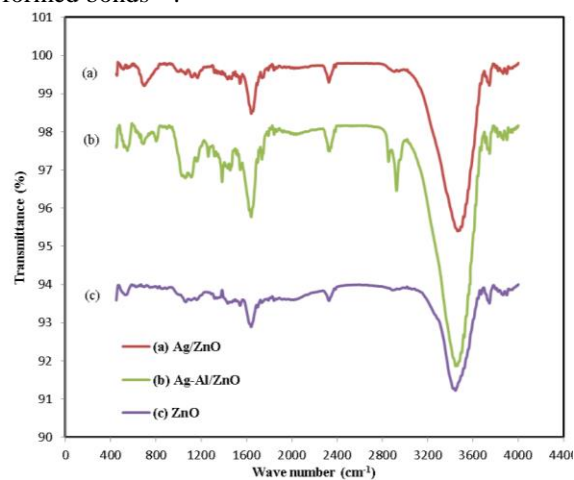


Figure 3. FTIR spectra of (a) Ag/ZnO (b) Ag-Al co doped ZnO (c) ZnO photocatalysts

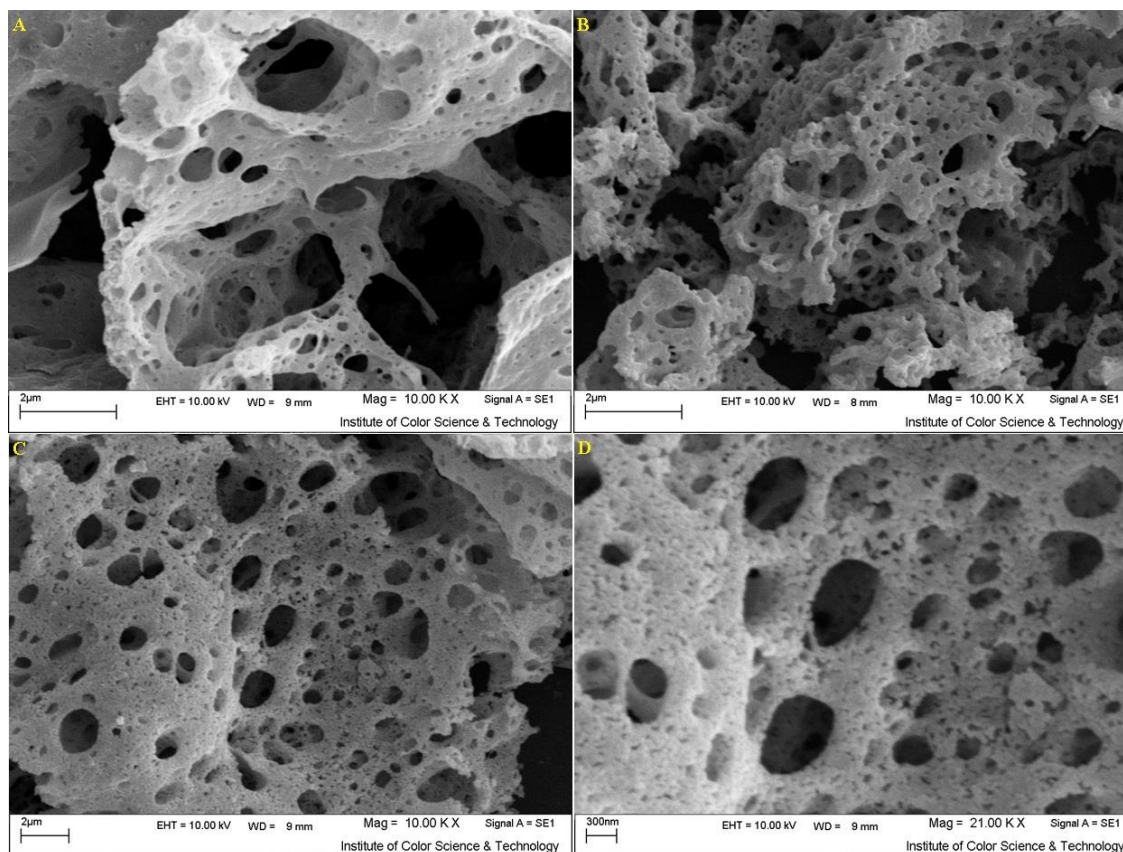


Figure 4. SEM images of ZnO (A), Ag modified ZnO (B) and Ag-Al co doped ZnO nanoparticles (C,D)

SEM Analysis

Figure 4A clearly shows the spongy morphology of ZnO catalyst before being doped with silver and aluminum. The SEM image of ZnO indicates that the clusters of particles stick together and make foam like structure with variable pore sizes which can be attributed to the type of combustion synthesis and the employed fuels mixtures (glycine and glucose). After

adding silver nitrate as precursors of silver to the prototype, the structure becomes more porous due to the decrease in fuel to oxidizer ratio and the generation of more combustion gases (Figure 4B). The morphology of the ZnO doped with 7% Ag and 3% Al is shown in Figure 4C and D. According to these figures the aluminium added to the structure of the catalyst causes a change in the hexagonal structure of ZnO. It can be noted that the Al

incorporation into the Ag/ZnO photocatalyst structure leads to a more uniform pore size distribution

Photocatalytic activity

Photodegradation of Reactive Blue 19 (RB19) was evaluated for the catalytic activity of ZnO in designed multi-layer cylindrical tubular reactor. The RB19 solution was made with a concentration of 10 - 40 mg/l dispersing 0.1 g/l ZnO in 1800 ml of the dye solution. Before the UV irradiation, a solution of dye and catalysts were circulated in the reactor in order to achieve the adsorption/desorption equilibrium. During a specific interval of time, 4 ml of solutions were immediately centrifuged for decolorization process evaluation by ultraviolet-visible (UV-Vis) absorption double beam spectrophotometer. It has been observed that less than 10 percent of RB19 decolorized in absence of UV radiation.

Effects of Ag and Al dopants on ZnO Photocatalytic Activity

Different molar ratios of Ag and Al have been examined to find the best amounts of Al and Ag as doping agents for ZnO photocatalyst. A fixed optimum operating condition (pH=7, 0.1 g. L⁻¹ photocatalyst dosage, 20 mg/L RB19 solution) is employed to investigate the effect of dopants. Photocatalytic activity of ZnO can be increased by addition of small amount of silver (3.5 mole% of Ag to ZnO). However, the maximum dye removal efficiency has been achieved at the silver loading of 7% as shown in Figure 5.

Upon UV irradiation, electrons are excited from the valence band of ZnO to its conduction band, leaving the corresponding holes in the valence band. Ag and Al dominate the electron capturing by increasing the electron and hole recombination time to enhance the separation efficiency of the photogenerated electrons and holes³⁶.

The photogenerated holes in the valence band of ZnO react with water and hydroxyl groups to form hydroxyl radicals, which leads to the photocatalytic oxidation of the dye. At the same time, the photogenerated electrons react with O₂ to form active oxygen species, which also participate in the photocatalytic oxidation of the dye.

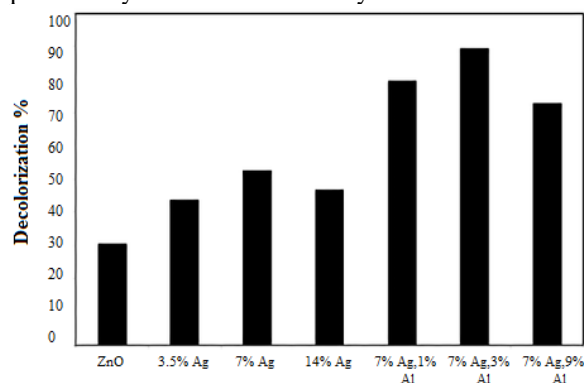


Figure 5. Modification of ZnO with different amounts of silver and aluminium (RB19 concentration = 20 (mg.L⁻¹), pH = 7, Time= 60 min)

Alumina particles have a significant role in improving the catalyst activity. It has been observed that the optimum amount of Al content for maximum catalytic activity is about 3 mol%. Photocatalytic activity is a strong function of the morphology and synthesis procedure²³. Next, the color degradation gradually decreases with increasing Al content to reach 8 mol %. This may be attributed more to the low(er) surface area of ZnO than to the incorporation of aluminum oxide clusters on the surface of zinc oxide, light adsorption of ZnO will be blocked by excessive aluminum. The enhancement of mesoporous Al_xO_y (x=1-2, y=1-5)- ZnO composite can be explained, that ZnO is the more photoactive than aluminum oxide for photocatalysis reactions. The addition of aluminum at low contents onto ZnO particles led to the better electrical properties effect and hence increased the separation efficiency of charge carriers⁴³.

Effect of Catalyst Dose

The photocatalytic efficiency of the synthesized Ag-Al /ZnO nanocatalyst at different catalyst loadings in the range of 0.025 - 0.15 g L⁻¹ is investigated. Experimental results show that the photodegradation efficiency is an increasing function of catalyst dosage up to 0.1 g L⁻¹ at 20 ppm RB19 solution. Decolorization efficiency increases to 80% during 60 minutes and then gradually reaches 90% after about 90 minutes. A further increase in the amount of catalyst beyond 0.1 g L⁻¹ does not have any significant effect on the degradation efficiency as shown in Figure 6.

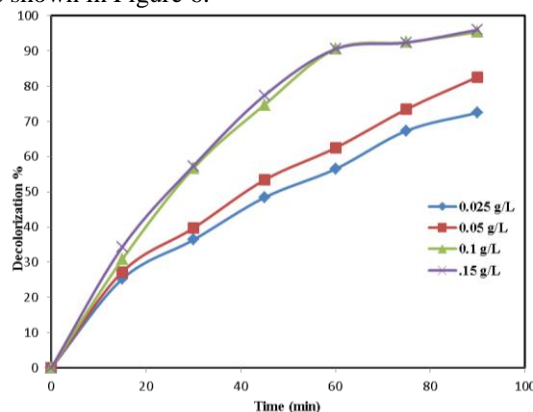


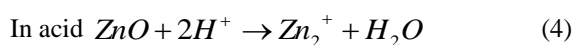
Figure 6. Decolorization versus time for different amounts of catalyst loading, Dye Solution= 20 (mg.L⁻¹), 7% mol Ag, 3% mol Al, pH = 7

An increase in the amount of loaded catalyst leads to an increase in the dye absorption efficiency on the surface of the catalyst. of alumina on ZnO particles increases the available surface due to the creation of more active sites³⁸. Reflected light from the surface of the catalyst causes more radiation scattering and increases the number of absorbed photons and generated hydroxyl radicals. One of the negative effects of more catalyst loading is the turbidity of the suspension which prevents transition of UV light in the reactor and retards the rate of decolorization^{33,34,44-46}.

Effect of pH

Because of the amphoteric behavior of semiconductor oxides, the effect of pH on the reaction rate is also studied in this work. Variation of pH affects the electron charge on the surface of the catalyst⁴⁷ and the dye degradation process under UV light irradiation⁴⁸. Decolorization of RB19 at different range of pH from 3 to 10 with a certain amount of catalyst (0.1 gr / lit) is investigated. Dye removal efficiency is quite low at pH=3 but for the pH range of 7- 9, the average decolorization rate is significantly enhanced to about 85% within one hour.

Zinc oxide which is an amphoteric oxide and can be hydrolyzed in water to produce hydroxide layers, reacts with H⁺ or OH⁻ according to the following equations^{33,46,49}:



There are electrostatic forces between the catalyst and the dye that are influenced by pH. So finding the pH at the zero charge (pH_{pzc}) is important where catalyst surface charge is positive, while at higher pH values the charge on the surface of the catalyst is negative due to the greater presence of OH⁻ Radicals⁵⁰. Thus there is a strong affinity between RB19 and catalyst surface for 3 < pH < 9 resulting in high removal efficiency of dye as shown in figure 7, the optimum pH range is between 7-9.

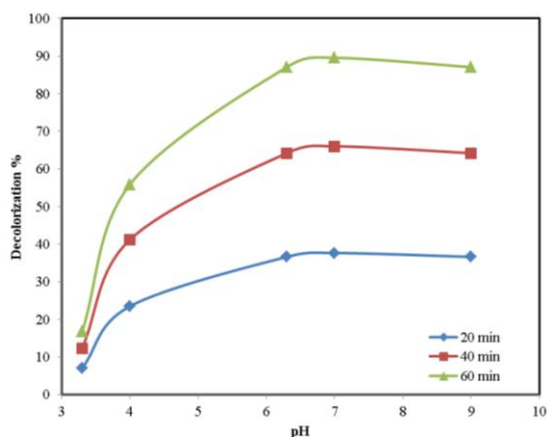


Figure 7. Effect of pH on decolorization of RB19 Dye Solution= 20 (mg.L⁻¹), Catalyst Dosage = 0.1 g/L, 7% mol Ag & 3% mol Al

Effect of dye Concentration

The impact of dye concentration on the rate of decolorization at different RB 19 solution concentrations from 10 ppm to 40 ppm with respect to the optimum catalyst structure (ZnO doped with 7 % mole Ag and 3% mole Al) and loading of 0.1 g L⁻¹ is investigated. Figure 8 shows the effect of initial dye concentration on photodegradation efficiency. It can be observed that as the dye concentration increases, the decolorization efficiency decreases.

Although an increase in the concentration leads to an increase in dye molecules adsorption on the surface of catalyst but less light reaches to the catalyst surface such that fewer active sites are available for the production of hydroxyl radicals. A similar behavior has been observed by Krishnakumar et al., 2011.

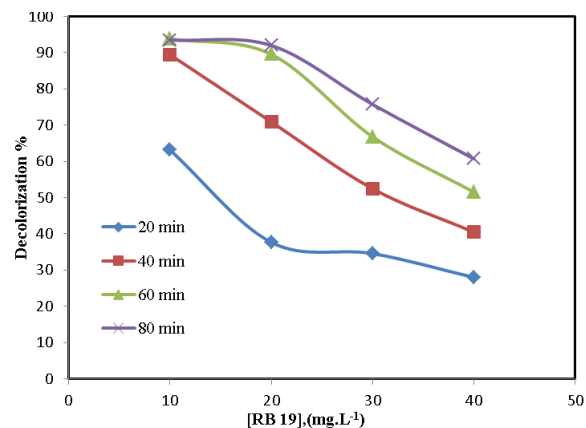


Figure 8. Decolorization of RB19 versus different dye concentrations Catalyst Dosage = 0.1 g/L, 7% mol Ag & 3% mol Al, pH=7

Mineralization

Mineralization of Reactive Blue 19 is studied by TOC analyzer and presented in Figure 9. It can be seen that the removal rate of organic compound is slower than that of the color as the organic chain takes 140 minutes to be dissociated while maximum decolorization efficiency of RB19 can be reached within 80 minutes. This may be due to the formation of intermediate components and competitive reactions with dye molecules⁵¹.

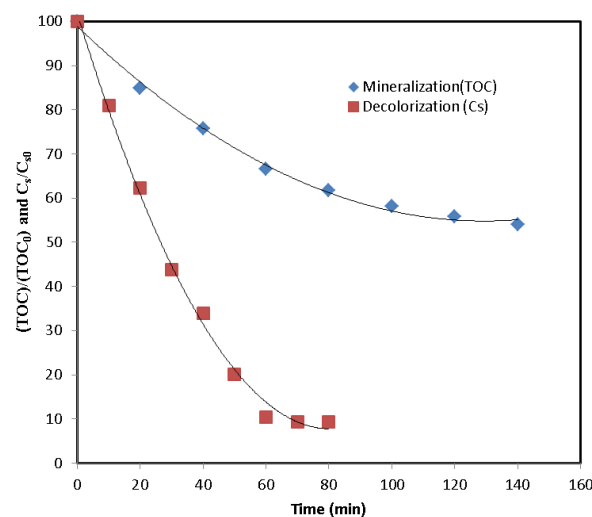


Figure 9. Normalized mineralization and decolorization efficiencies of RB19 versus time Dye Solution= 20 (mg.L⁻¹), Catalyst Dosage = 0.1 g/L, 7% mol Ag and 3% mol Al

Kinetic Studies

The photocatalytic degradation of organic materials can be described by Langmuir adsorption kinetics equation as follows:

$$r = \frac{dC}{dt} = \frac{kKC}{1+KC} \quad (6)$$

Eq. (6) can be simplified to the pseudo-first order kinetic model:

$$\ln \frac{C_0}{C} = kKt = K_{app}t \quad (7)$$

Where C_0 and C are initial concentration of the dye (mol/l) and concentration of the dye at time t (mol/l) respectively; t is irradiation time (min), k and K are reaction rate constant ($\text{mol.l}^{-1}.\text{min}^{-1}$) and

adsorption coefficient of the dye onto the photocatalyst particle (l/mol) respectively, K_{app} is the pseudo reaction rate constant (min^{-1}). Decolorization of RB19 with modified ZnO (7% mole Ag and 3% mole Al) can be described with a pseudo first order kinetic model. Figure 10 represents a linear relationship between $\ln(C_0/C)$ and time. Figure 11 represents the pseudo-first-order rate constants for dye removal at different molar concentrations of aluminum and silver. Presented results in Table 1 show the rate constants at different concentrations of RB19 indicating that the dye removal efficiency of the modified ZnO (3% Al and 7% Ag) is three times higher than that of Ag doped ZnO and six times higher than that of ZnO.

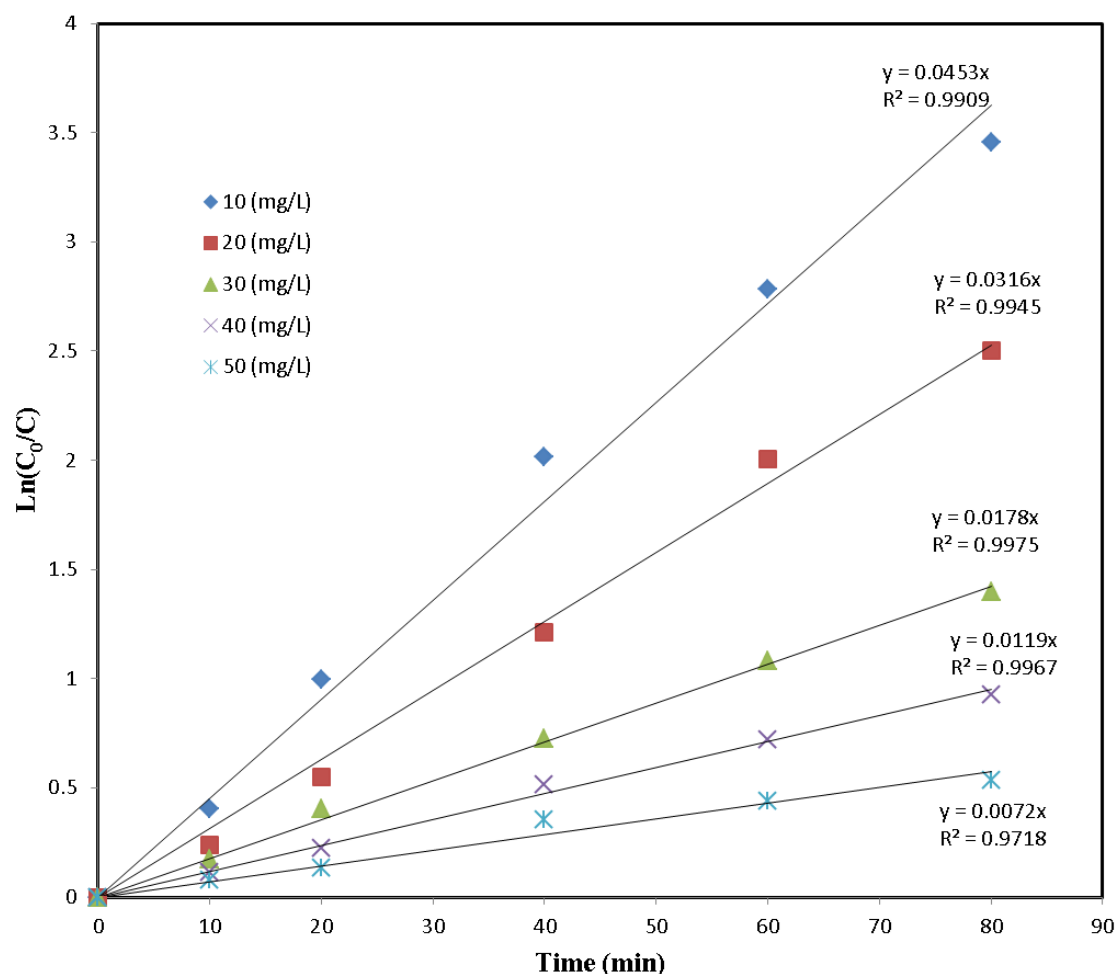


Figure 10. Kinetic study of RB19 decolorization process (Ag-Al/ZnO Dosage = 0.1 g/L, 7% mol Ag & 3% mol Al)

Table 1 : Pseudo first order rate constant for different RB19 concentrations

(Ag-Al/ZnO Dosage = 0.1 g/L, 7% mol Ag & 3% mol Al)					
	10 ppm	20 ppm	30 ppm	40 ppm	50 ppm
K_{app} (min^{-1})	0.0453	0.0316	0.0178	0.0119	0.0072
R^2	0.9909	0.9945	0.9975	0.9967	0.9718

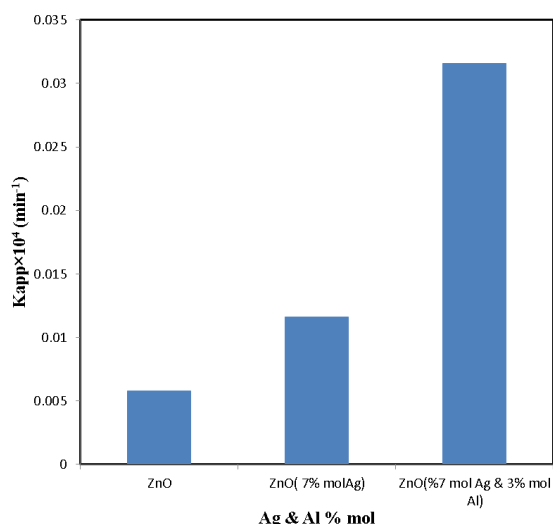


Figure 11. Pseudo first order rate constant for ZnO photocatalyst with different Ag and Al loadings (Dye Solution= 20 (mg.L⁻¹), Catalyst Dosage = 0.1 g/L)

Energy Consumption Determination

The photocatalytic wastewater treatment is a process that consumes electrical energy. This can be an important factor to determine operation costs.

Table2 (3) : Electrical energy per order (EE/O) and total cost for UV/catalyst process (Ag-Al/ZnO Dosage = 0.1 g/L, 7% mol Ag & 3% mol Al)

Dye concentration (ppm)	Rate Constant (min ⁻¹)	EE/O (kWh m ⁻¹ order ⁻¹)	Total Cost (USD)
10	0.0453	6.30	0.0819
20	0.0316	4.3952	0.0984
30	0.0178	7.8027	0.1856
40	0.0119	11.6713	0.2389
50	0.0072	19.2901	0.2507

As shown, an increase in dye concentration leads to longer reaction time and more UV energy demand such that the rate of reaction decreases and the costs of photocatalytic reaction increase. Figure 12 compares the required electrical energy (EE/O) for RB19 removal using different nanophotocatalyst. Also the electrical energy consumptions for removal of different dyes using different nanocatalysts are compared in Figure 13 at a fixed initial dye concentration of 50 ppm. As shown in Figures 12 and 13, the required electrical energy for dye removal by the synthesized Ag-Al/ZnO nano-photocatalyst used in this work is always much lower as compared to the other available alternatives⁵³⁻⁵⁷.

The volumetric electrical energy consumption per order (EE/O) and the electrical energy consumption cost⁵² are determined according to the following equations:

$$EE/O = \frac{P \times t \times 1000}{V \times 60 \times \log(C_i / C_f)} \quad (8)$$

$$\ln\left(\frac{C_i}{C_f}\right) = K_{app} \times t \quad (9)$$

EE/O (kWh m⁻³order⁻¹) shows the electrical energy requirement for reducing pollution level up to 90% in 1 m³ of aqueous solution. In this equation P is the rated power (kW) of the AOP system, t is the irradiation time (min), V is the volume (L) of the water in the reactor, C_i and C_f are the initial and final pollutant concentrations respectively and K_{app} is the pseudo-first-order rate constant (min⁻¹).

The electrical energy costs by using the synthesized nano-photocatalyst at different dye concentrations have been determined according to electrical energy price (0.013 USD/KWh in September 2013) and displayed in Table 2.

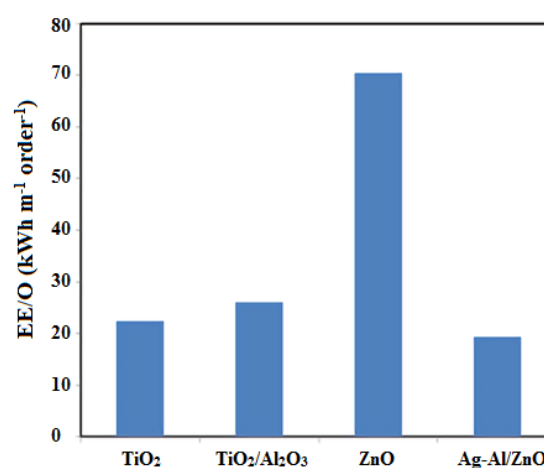


Figure 12. EE/O for RB19 photodecolorization.

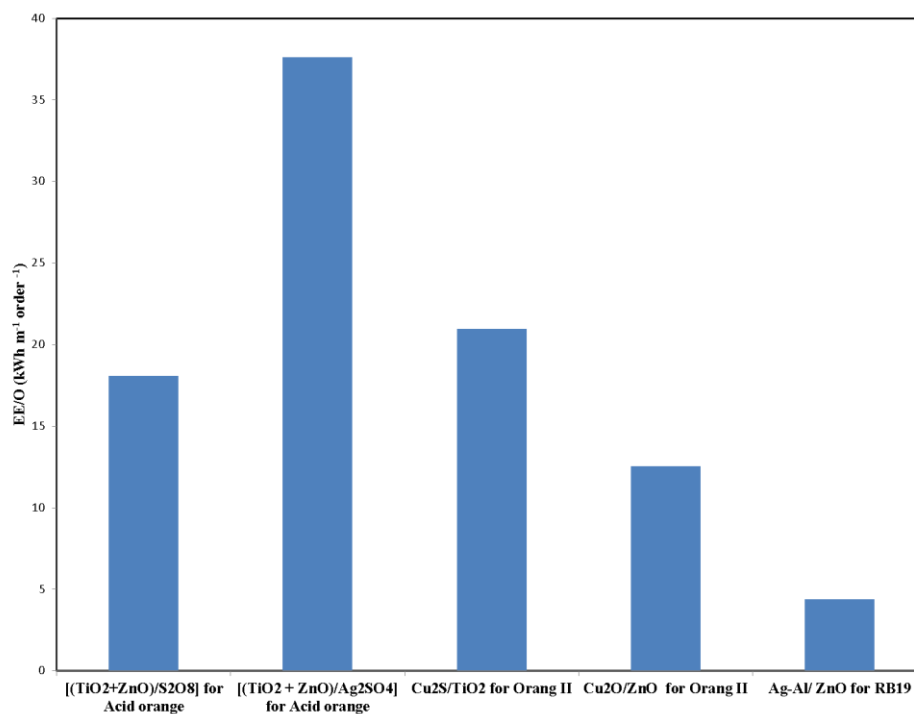


Figure 13. EE/O for photo-decolorization with different photocatalyst at the same concentration of dyes (50 ppm).

Conclusions

In this work the Ag-Al/ZnO nano-photocatalyst is synthesized by using microwave assisted combustion technique and characterized by different Hi-Tech equipments. The photocatalytic performance of the synthesized Ag-Al/ZnO nano-photocatalyst is evaluated by photo-degradation of RB19 under UV radiation in a newly designed multi-layer cylindrical tubular reactor. Kinetic studies of synthesized photocatalyst show that the decolorization process follows a pseudo first order kinetics. The experimental observations confirm that the synthesized Ag-Al/ZnO nano-photocatalyst has much more photocatalytic activity as compared to the other available ZnO/catalyst combinations. The best operating performance is obtained at the pH of 7, photocatalyst dosage of 0.1 g/L and RB19 solution concentration of 20 mg/L. The advantage of the synthesized nano-photocatalyst in this work over the other available ones regarding electrical energy consumption is clearly demonstrated. The synthesized nano-photocatalyst and the new fabricated multi-layered cylindrical reactor can have potential applications for deep removal of similar dyes from industrial wastewaters.

References

- 1- A. Aleboyeh, M. E.Olya, H. Aleboyeh, Electrical energy determination for an azo dye decolorization and mineralization by UV/H₂O₂ advanced oxidation process. *J. Chem. Eng.* 137 **2008**, 518-524.
- 2- S. Fettouche, M. Tahiri, R. Madhouni, O. Cherkaoui, Removal of Reactive Dyes From Aqueous Solution by Adsorption onto Alfa Fibers powder. *J. Mater. Environ. Sci.* 6, **2015**, 129-137
- 3- Y. He, J.F. Gao, F.Q. Feng, C. Liu, Y.Z. Peng, S.Y. Wang, The comparative study on the rapid decolorization of azo, anthraquinone and triphenylmethane dyes by zero-valent iron. *J. Chemical Engineering* 179 , **2012**, 8- 18.
- 4- S. Dutta, S.A. Parsons, C. Bhattacharjee, P. Jarvis, S. Datta, S. Bandyopadhyay, Kinetic study of adsorption and photo-decolorization of Reactive Red 198 on TiO₂ surface. *J. Chemical Engineering* 155, **2009**, 674-679. M.
- 5- A. Pirkarami, M.E. Olya, N. Yousefi Limaee, Decolorization of azo dyes by photo electro adsorption process using polyaniline coated electrode. *J. Progress in Organic Coatings* 76, **2013**, 682- 688
- 6- S. Mohammadi-Aghdam, R. Marandi, M.E. Olya, A.A. Mehrdad Sharif, Kinetic modeling of BB41 photocatalytic treatment in a semibatch flow photoreactor using a nano composite film. *J. Saudi Chemical Society* 20, **2013**, 103-109.
- 7- R. Marandi, M.E. Olya, B. Vahid, M. Khosravi, M. Hatami, Kinetic Modeling of Photocatalytic Degradation of an Azo Dye Using Nano-TiO₂/Polyester. *J. Environmental Engineering Science.* 25, **2012**, 108-119.
- 8- C. Karunakaran, V. Rajeswari, P. Gomathisankar, Optical, electrical, photocatalytic, and bactericidal properties of microwave synthesized nanocrystalline

- AgeZnO and ZnO. *J. Solid State Sciences* 13, **2011**, 923-928.
- 9- M.Pudukudy, Z.Yaakob, R.Rajendran, T.Kandaramath, Photodegradation of methylene blue over novel 3D ZnO micro-flowers with hexagonal pyramid-like petals. *J.Reac Kinet Mech Cat* 112, **2014**, 527-542.
- 10- Y. Lou, S. Yuan, Y. Zhao, P. Hub, Z. Wang, M. Zhang, L. Shi, D. Li, A simple route for decorating TiO₂ nanoparticle over ZnO aggregates dye-sensitized solar cell. *J. Chemical Engineering* 229, **2013**, 190-196.
- 11- J. Iqbal, T. Jana, M. Ismail, N. Ahmada, A. Arifa, M. Khana, M. Adila Sami-ul-Haqa, A. Arshada, Influence of Mg doping level on morphology, optical, electrical properties and antibacterial activity of ZnO nanostructures. *J. Ceramics International in Press*, **2013**.
- 12- G. Li, X. Zhu, X. Tang, W. Song, Z. Yang, J. Dai, Y. Sun, X. Pan, S. Dai, Doping and annealing effects on ZnO:Cd thin films by sol-gel method. *J.Alloys and Compounds* 509, **2011**, 4816-4823
- 13- S. Ameen, M. Shaheer Akhtar, H. K.Seo, Y. Soon Kim, H. Shik Shin, Influence of Sn doping on ZnO nanostructures from nanoparticles to spindle shape and their photoelectrochemical properties for dye sensitized solar cells. *J. Chem. Eng.* 187, **2012**, 351-356
- 14- L. Arda, M. Acikgoz, Z.K. Heiba, N. Dogan, D. Akcan, O. Cakiroglu, Synthesis, characterization and ESR studies of powder Zn_{0.95-x}Mg_{0.05}Al_xO (x=0, 0.01, 0.02, 0.05, and 0.1) nanocrystals. *Solid State Comm.* 170, **2013**, 14-18
- 15- W. Xie, Y. Li, W. Sun, J. Huang, H. Xie, X. Zhao, Surface modification of ZnO with Ag improves its photocatalytic efficiency and photostability, *J. Photochemistry and Photobiology A: Chemistry.* 216, **2010**, 149-155.
- 16- Y. Li, J. Meng, Al-doping effects on structure and optical properties of ZnO nanostructures. *Materials Letters* 117, **2014**, 260-262.
- 17- D. Fang, K. Lin, T. Xue, C. Cui, X. Chen, P. Yao, H. Li, Influence of Al doping on structural and optical properties of Mg-Al co-doped ZnO thin films prepared by sol-gel method. *Journal of Alloys and Compounds* 589, **2014**, 346-352.
- 18- C. Aydın, M.S. Abd El-sadek, K. Zheng, I.S. Yahia, F. Yakuphanoglu, Synthesis, diffused reflectance and electrical properties of nanocrystalline Fe-doped ZnO via sol-gel calcination technique. *J. Optics & Laser Technology* 48, **2013**, 447-452.
- 19- H. J.Son, K.A. Jeon, C.E. Kim, J.H. Kim, K.H. Yoo, S.Y. Lee, Synthesis of ZnO nanowires by pulsed laser deposition in furnace. *Optics & Laser Technology* 48, **2013**, 447-452.
- 20- Q. Simon, D. Barreca, D. Bekermann, A. Gasparotto, E.C. Maccato, V. Gombac, P. Fornasiero, O.I. Lebedev, S. Turner, A. Devi, R.A. Fischer, G.V. Tendeloo, Plasma-assisted synthesis of Ag/ZnO nanocomposites: First example of photo-induced H₂ production and sensing. *J. Hydrogen Energy* 36, **2011**, 15527-15537.
- 21- S. Mitra, K. Sridharan, J. Unnam, K. Ghosh, Synthesis of nanometal oxides and nanometals using hot-wire and thermal CVD. *J.Thin Solid Films* 516, **2008**, 798-802.
- 22- A.A. Ismail, A. El-Midany, E.A. Abdel-Aal, H. El-Shall, Application of statistical design to optimize the preparation of ZnO nanoparticles via hydrothermal technique. *J. Materials Letters* 59, **2005**, 1924-1928.
- 23- M.Pudukudy, Z.Yaakob, Hydrothermal synthesis of mesostructured ZnO micropylamids with enhanced photocatalytic performance. *J.Superlattices and Microstructures* 63, 2013, 47-57.
- 24- M.Pudukudy, Z.Yaakob, Facile Synthesis of Quasi Spherical ZnO Nanoparticles with Excellent Photocatalytic Activity. *J.Clust Sci* **2014**, 1572-8862.
- 25- M.Pudukudy, Z.Yaakob, Facile solid state synthesis of ZnO hexagonal nanogranules with excellent photocatalytic activity. *J. Applied Surface Science* 292, **2014**, 520- 530
- 26- M.Pudukudy, A.Hetieqa, Z.Yaakob, Synthesis, characterization and photocatalytic activity of annealing dependent quasi spherical and capsule like ZnO nanostructures. *J. Applied Surface Science* 319, **2014**, 221-229.
- 27- M.Pudukudy, Z.Yaakob. Simple chemical synthesis of novel ZnO nanostructures: Role of counter ions. *J.Solid State Sciences* 30,**2014**,78-88.
- 28- Z. Chen, Y. Yanc, Microwave induced solution combustion synthesis of nano-sized phosphors. *J. Alloys and Compounds* 473, **2009**, 13-16.
- 29- V. Jeena, S.R. Ross, An environmentally friendly, cost effective synthesis of quinoxalines: the influence of microwave reaction conditions. *J.Tetrahedron Letters* 55, **2014**, 642-645.
- 30- M.H. Eman, A. Sobhi, A. Gomha, F. Thoraya, Multicomponent reactions for synthesis of bioactive polyheterocyclic ring systems under controlled microwave irradiation. *Arabian Journal of Chemistry Available online* 25 November, **2013**.
- 31- G.Donati, R.Paludetto, Batch and semibatch catalytic reactors (from theory to practice) *J. Catalysis Today* 52, **1999**, 183-195.
- 32- M.N. Chong, B. Jin, C.W.K. Chow, C. Saint, Recent developments in photocatalytic water

- treatment technology: A review. *J. water research* 44, **2010**, 2997-3027.
- 33- C. H. Wu, Effects of sonication on decolorization of C.I. Reactive Red 198 in UV/ZnO system. *J. Hazardous Materials* 153, **2008**, 1254-1261.
- 34- B. Krishnakumar, M. Swaminathan, Influence of operational parameters on photocatalytic degradation of a genotoxic azo dye Acid Violet 7 in aqueous ZnO suspensions. *J. Spectrochimica Acta Part A* 81, **2011**, 739-744.
- 35- M. Ahmad, E. Ahmedb, Y. Zhang, N.R. Khalid, J. Xu, M. Ullah, Z. Hong, Preparation of highly efficient Al-doped ZnO photocatalyst by combustion synthesis. *J. Current Applied Physics* 13, **2013**, 697-704.
- 36- L. Wu, Y. Wu, Preparation of ZnO Nanorods and optical characterizations. *J. Physica E: Low-dimensional Systems and Nanostructures* 28, **2005**, 76-82.
- 37- Y.J. Kwon, K.H. Kim, C.S. Lim, Characterization of ZnO nanopowder synthesized by the polymerized complex method via an organochemical route. *J. Ceram Proc Res*, 3, **2002**, 146-149.
- 38- R.F. Silva, M.E.D. Zaniquelli, Morphology of nanometric size particulate aluminium-doped zinc oxide films. *J. Colloid Surf Physicochem Eng Aspect*, 198, **2013**, 551-558.
- 39- W. Tang, D.C. Cameron, Electroluminescent zinc sulphide devices produced by sol-gel processing. *J. Thin Solid Films* 280, **1996**, 221.
- 40- A. H.Shah, E. Manikandan, A. M.Basheer, V. Ganesan, Enhanced Bioactivity of Ag/ZnO Nanorods-A Comparative Antibacterial Study. *J. Nanomed Nanotechol* 4, **2013**, 2-6.
- 41- A.Ortiz, J.C. Alonso, V. Pankov, A. Huanosta, E. Andrade, Characterization of amorphous aluminum oxide films prepared by the pyrosol process *Thin. J. Solid Films* 368, **2000**, 74.
- 42- B. Divbanda, M. Khatamian, G.R. Kazemi Eslamian, M. Darbandi, Synthesis of Ag/ZnO nanostructures by different methods and investigation of their photocatalytic efficiency for 4-nitrophenol degradation. *J. Applied Surface Science* 284, **2013**, 80- 86.
- 43- D.R.Sahu, S.Y.Lin, J.L.Huang, Deposition of Ag-based Al-doped ZnO multilayer coatings for the transparent conductive electrodes by electron beam evaporation. *J.Solar Energy Materials & Solar Cells*, 91, **2007**, 851-855.
- 44- A. Aprilia, P. Wulandari, R. Hidayat, A. Fujii, M. Ozaki, Influences of dopant concentration in sol-gel derived AZO layer on the performance of P3HT:PCBM based inverted solar cell. *Solar Energy Materials & Solar Cells* 111, 181, **2013**,188.
- 45- T. Hajizadegan, M. Jafari, M. Rashidzadeh, A. Saffar-Teluri, A high activity adsorbent of ZnO-Al₂O₃ nanocomposite particles: Synthesis, characterization and dye removal efficiency. *J. Applied Surface Science* 276, **2013**, 317-322.
- 46- G.L. PUMA, Dimensionless Analysis of Photocatalytic Reactors Using Suspended Solid Photocatalysts. *J.Chemical Engineering Research and Design* 83, **2005**, 820-826.
- 47- N. Modirshahla, A. Hassani, M.A. Behnajady, R. Rahbarfam, Effect of operational parameters on decolorization of Acid Yellow 23 from wastewater by UV irradiation using ZnO and ZnO/SnO₂ photocatalysts. *J. Desalination*. 271, **2011**, 187-192.
- 48- B. Gözmen, M. Turabik, A. Hesenov, Photocatalytic degradation of Basic Red 46 and Basic Yellow 28 in single and binary mixture by UV/TiO₂/periodate system. *J. Hazardous Materials*. 164, **2009**, 1487-95.
- 49- C. E. Housecroft, S.A. Gharpe, *Inorganic Chemistry* (2nd ed.). Prentice Hall. **2004**, pp. 173-4.
- 50- M.M. Ba-Abbad, A.A.H. Kadhum, A.B. Mohammad, M.S. Takriff, K. Sopian, Visible light photocatalytic activity of Fe(3+)-doped ZnO nanoparticle prepared via sol-gel technique. *J. Chemosphere*. 91, **2013**, 1604-11.
- 51- P. Canizares, M. Hernandez-Ortega, M.A. Rodrigo, C.E. Barrera-Diaz, G. Roa-Morales, C. Saez, A comparison between Conductive-Diamond Electrochemical Oxidation and other Advanced Oxidation Processes for the treatment of synthetic melanoidins. *J. Hazardous aterials* 164, **2009**, 120-125
- 52- M.E. Olya, A. Pirkarami, M. Soleimani, M. Bahmaei, Photoelectrocatalytic degradation of acid dye using Ni-TiO₂ with the energy supplied by solar cell: Mechanism and economical studies. *J. Environmental Management* 121, **2013**, 210-219.
- 53- J. Ulson, J. Alison, D.F. Ollis, Kinetics of dye decolorization in an air-solid system. *J.Applied Catalysis B: Environmental* 65, **2006**, 315-325.
- 54- N. Helaili, Y. Bessekhoud, A. Bouguelia, M.Trari, p-Cu₂O/n-ZnO heterojunction applied to visible light Orange II degradation. *J. Solar Energy* 84, **2010**, 1187-1192.
- 55- C. Lizama, J. Freer, J. Baeza, H.D. Mansilla, Optimized photodegradation of Reactive Blue 19 on TiO₂ and ZnO suspensions. *J.Catalysis Today* 76, **2002**, 235-246
- 56- W.A. Sadik, Decolourization of an Azo Dye by Heterogeneous Photocatalysis. *J.rocess Safety and Environmental Protection* 85, **2007**, 515-520.
- 57- Y. Bessekhoud, R. Brahimia, F. Hamdinia, M. Trari, Cu₂S/TiO₂ heterojunction applied to visible light Orange II degradation. *J. Photochemistry and Photobiology A: Chemistry* 248, **2012**, 15-23.